Instrument Science Report WFC3 2013-011

UVIS PSF SPATIAL & TEMPORAL VARIATIONS

E. Sabbi & A. Bellini

June 25, 2013

ABSTRACT

Observations of the globular cluster ω Centauri in the filter F606W were used to characterize the impact of telescope breathing on the UVIS PSF as a function of position across the detector. Our study suggests that these variations can be well characterized using data from the archive and that it is possible to correct empirical and/or theoretical PSF models by taking into account the value of the telescope focus at the moment of the observations.

Introduction

As for several other *Hubble Space Telescope (HST)* instruments, flat-fields for the UVIS channel of the Wide Filed Camera 3 (WFC3) were acquired from the ground under thermal vacuum conditions (Sabbi et al 2008). These data provide a good representation of the detector pixel-to-pixel variation and are still at the foundation of the reference files used today for the on-orbit data.

Previous experience with other *HST* instruments, such as the Advanced Camera for Surveys (ACS) and the Space Telescope Imaging Spectrograph (STIS), showed that it is very difficult to accurately reproduce the Optical Telescope Assembly with an optical stimulus (i.e. CASTLE) to simulate the sky illumination of an instrument. As a result, ground-based flat-fields differ from the on-orbit data on large spatial scales, and it is necessary to apply additional corrections to ensure the spatial independency of the photometry.

During the Servicing Mission Observatory Verification (SMOV), observations of the two globular clusters 47 Tucanae and ω Centauri were used to validate the quality of UVIS

flat fields. The photometric analysis of this dataset showed local variations in magnitude of the order of 1.5 - 4.5% from the optical to the UV, with higher uncertainties at shorter wavelengths (Sabbi 2009a). A detailed description of all the steps required to improve the quality of the UVIS flats can be found in Mack et al. (2013).

Two calibration programs (CAL-11911 and CAL-12339; PI Sabbi) were designed to observe the globular cluster ω Centauri in 10 broad-band filters and correct the UVIS flats for the low-frequency structures caused by the difference between the optical stimulus CASTE and the on-orbit data. Several factors contributed in selecting ω Centauri as the target to improve the flat-fields (Sabbi et al. 2009). First of all, the cluster hosts a large number of blue horizontal branch and red giant branch stars, and therefore can be used to uniformly sample the flat-field low-frequency structures over the entire wavelength range covered by UVIS. More importantly, the core of ω Centauri is wide and flat, and the lack of a stellar density gradient guarantees each portion of the detector to be equally weighted, minimizing the introduction of artificial structures.

The UVIS point-spread function (PSF) changes both as a function of position across the detector and telescope breathing. For example, in the upper-left corner of the detector the brightness of a star measured with a 5 pixel radius aperture shows variations in photometry of the order of 3 to 7% from one exposure to another (Sabbi 2009b). This behavior complicates the analysis of low frequency structures: on one hand a large number of stars is required to statistically measure the local variations in the photometry introduced by the flat fields (hence the choice of a stellar field as rich as the core of ω Centauri), on the other hand it is important to measure the flux of the stars within an aperture larger than 8-9 pixels, to overcome breathing and distortion variations.

Here we discuss how the PSF spatially changes with the telescope focus, and investigate if it is possible to predict the PSF behavior.

Data

The globular cluster ω Centauri was observed with the broad-band UVIS filters F225W, F275W, F336W, F390W, F438W, F555W, F606W, F775W, F814W, and F850LP during Cycle 17 (CAL-11911; PI Sabbi) and Cycle 18 (CAL-12339, PI Sabbi) as part of the extensive calibration campaign of the WFC3/UVIS channel. The data were used to derive the low-frequency correction (L-flat) to improve the quality of the UVIS flat-fields. In addition the same datasets were used to derive the geometric-distortion correction for UVIS data (Bellini & Bedin 2009, Bellini e al. 2010, Kozurina-Platais et al. 2009, Kozurina-Platais & Petro 2012). Figure 1 shows how the PSF changes as a function of wavelength in 9 UVIS broad-band filters, from the near UV, where the PSF is sharper, to the near IR, where it is possible to distinguish the first Airy ring.

List of Observations

To characterize UVIS PSF temporal variations we focus our analysis on the F606W filter. A total of 36 exposures were acquired between January 2010 and February 2011 in this filter. The observations were organized in four different epochs. During each epoch 9x40 s exposures were acquired, each shifted in RA and/or in Dec by ¼ of the UVIS field of view. Each epoch is rotated by ~90° with the respect to the previous one.

Table 1 summarizes the list of the observations. Five out of six of the observations acquired on April 29, 2010 and one of the observations acquired on February 14, 2011 are degraded because of the loss of the Guide stars. These observations are stricken through in Table 1, and will not be further discussed in this ISR.

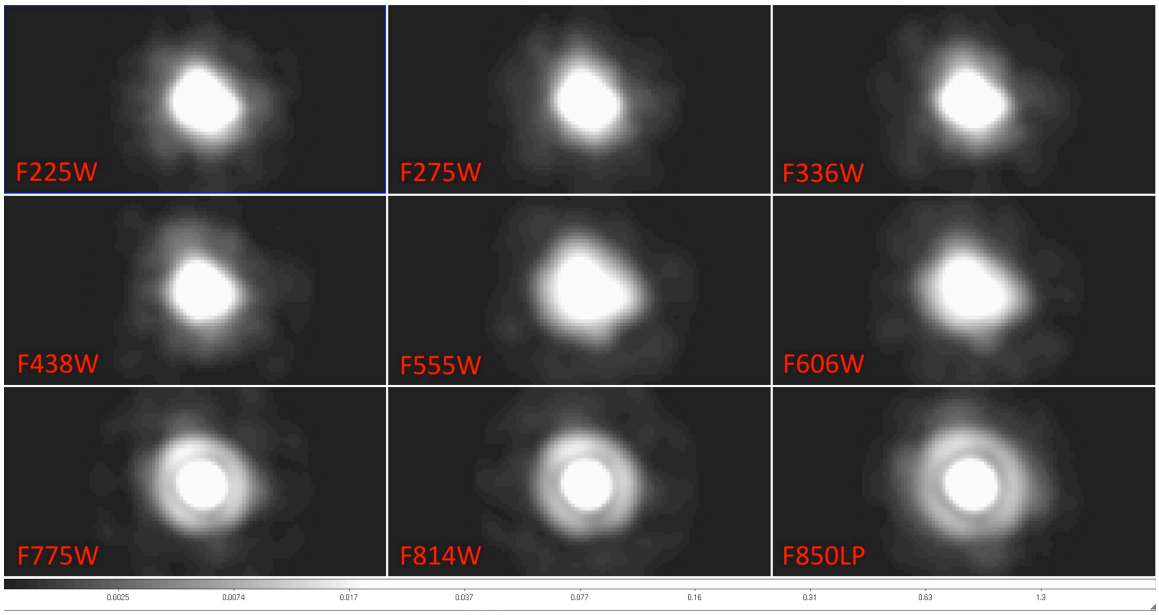

Figure 1: Example of PSF for the filters F225W, F275W, F336W, F438W, F555W, F606W, F775W, F814W, and F850LP. Images are shown in a logarithmic scale to show both the wings and the core of the PSFs.

Image name	Proposal ID	OBS date	PAV3
ibc301qrq	11911	14/01/10	105.0003
ibc302ivq	11911	12/01/10	105.0108
ibc302j0q	11911	12/01/10	105.0169
ibc302j2q	11911	12/01/10	105.0064
ibc302j7q	11911	12/01/10	104.9959
ibc302jcq	11911	12/01/10	104.9898
ibc303n1q	11911	13/01/10	104.9837
ibc303n9q	11911	13/01/10	104.9942
ibc303nbq	11911	13/01/10	105.0047
ibc304v3q	11911	29/04/10	199.9971
~~ibc305ynq~~	~~11911~~	~~29/04/10~~	~~200.0023~~
~~ibc305ysq~~	~~11911~~	~~29/04/10~~	~~199.9913~~
~~ibc305yuq~~	~~11911~~	~~29/04/10~~	~~199.9861~~
~~ibc305yzq~~	~~11911~~	~~29/04/10~~	~~199.981~~
~~ibc305z4q~~	~~11911~~	~~29/04/10~~	~~199.992~~
ibc306q7q	11911	28/04/10	200.0029

ibc306qqq	11911	28/04/10	200.0081
ibc306qsq	11911	28/04/10	200.0132
ibc307qyq	11911	04/07/10	279.9995
ibc307raq	11911	04/07/10	279.9895
ibc307rgq	11911	04/07/10	279.9825
ibc307rpq	11911	04/07/10	279.9925
ibc307sjq	11911	04/07/10	280.0024
ibc307soq	11911	04/07/10	280.0093
ibc307sqq	11911	04/07/10	280.0163
ibc307stq	11911	04/07/10	280.0064
ibc307syq	11911	04/07/10	279.9965
~~ibla01doq~~	~~12339~~	~~14/02/11~~	~~139.9986~~
ibla01drq	12339	14/02/11	140.0107
ibla01dwq	12339	14/02/11	140.0097
ibla01dyq	12339	14/02/11	139.9976
ibla01e6q	12339	14/02/11	139.9865
ibla01e8q	12339	14/02/11	139.9875
ibla01ebq	12339	14/02/11	139.9996
ibla01egq	12339	14/02/11	140.0117
ibla01e1q	12339	14/02/11	139.9855

Table 1: List of the observations acquired during Cycle 17 and 18 in the F606W filter to derive the L-flat correction. The image name is listed in column 1, column 2 reports the proposal ID, the observing date is in column 3, and column 4 provides the telescope roll angle (PA_VA3).

Data Analysis

As for other *HST* instruments, the PSF of UVIS varies with wavelengths, position on the detector, and time. Variations within the field of view are caused by a combination of defocus, coma, astigmatism, spherical aberration, and charge diffusion, while the main sources of temporal variation are the focus change and the spacecraft jittering during the exposures.

In order to characterize the spatial and temporal variation of the PSF we used a code based on the software img2xym_WFI (Anderson et al. 2006) and adapted to UVIS data by Bellini & Bedin (2009), to create a grid of empirical PSFs for each single image. This approach allowed us to reconstruct the spatial variation of the encircled energy distribution for a specific observation.

Spatial Variations

In general, field-dependent variations in the WFC3/UVIS channel are less severe than in other *HST* cameras, however core-width and elipticity variations across the field are large enough to be a concern in the case of small radii (r<10 pixel) aperture photometry. Therefore it is important to assume a spatially-variable PSF when computing a PSF

model for the PSF-fitting photometry. The change in the detector thickness (Wong 2010) and the tilt of the camera with the respect to the focal plane are the major causes of variation of the FWHM across the UVIS field of view.

For each F606W image we created a 9x10 grid of empirical PSFs. Figure 2 shows the residuals between the grid of PSF models for one image and a spatially constant PSF derived for the same image. While the residuals are generally small (less than 1%), in the upper-left and lower-right corners the PSFs are broader, and ~12-15% of the flux is pushed from the central peak to the wings. As a result stars in these reigons will appear fainter than the average if their magnitude is measured using a small (r<10 pixel) photometry in using a small aperture photometry, stars will be . In the lower half of the detector (between 2200<X<3000 pixels, in the region of the "happy bunny", named for the shape of the fringing pattern), the PSF is sharper than average, and the residuals show an excess of 15-17% in the peak compared to the average PSF, thus a small aperture photometry will give a magnitude higher than the average.

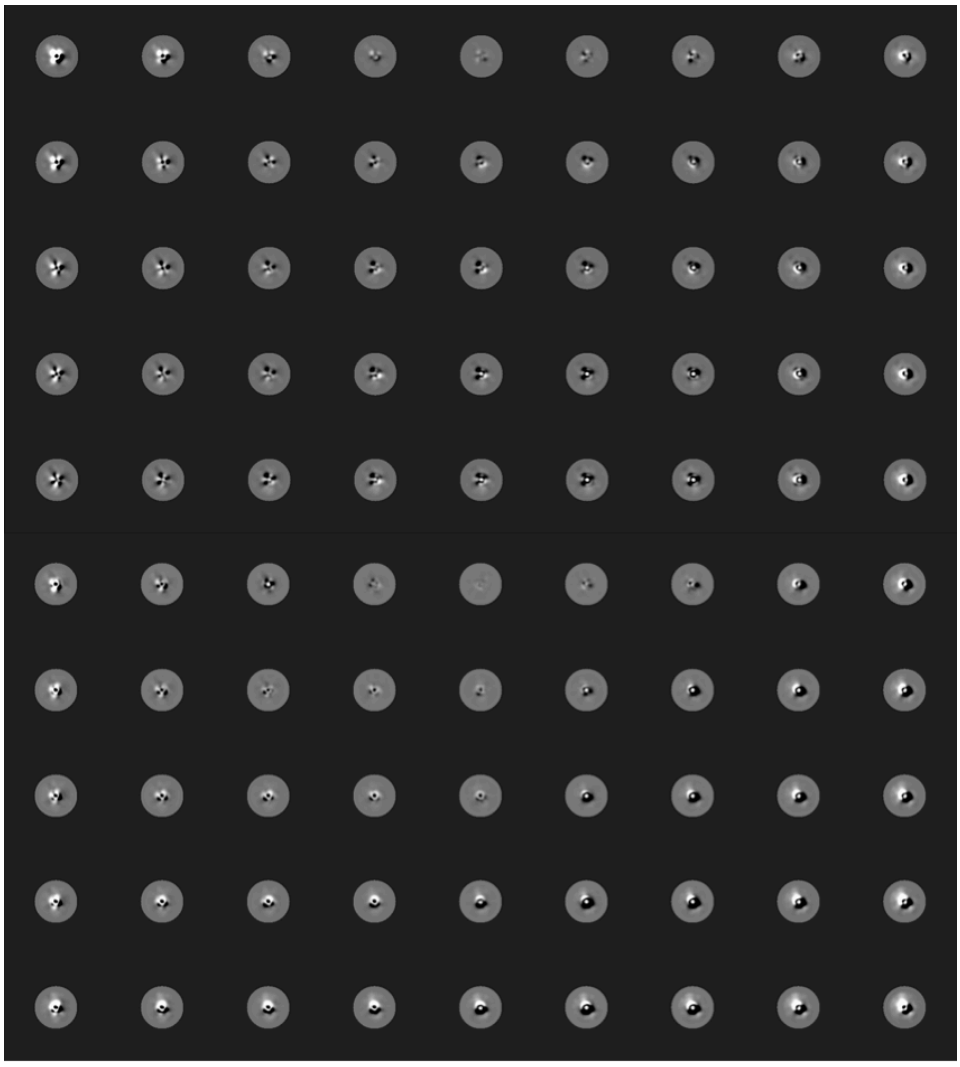

Figure 2: Residuals between a 9x10 grid of empirical PSF and the average PSF. USIV chip 1 is on top and chip 2 is on the bottom. White represents an excess and black a deficit of flux of the local PSF compared to the average one.

Temporal Variations

HST is subject to two heating cycles during its orbit around the Earth. The first heating cycle occurs when the telescope is illuminated by the Sun (day). The amount of heat that HST receives during the day depends on the orientation of the spacecraft with respect to the Sun and on its roll angle.

The second cycle occurs when the Earth occults the Sun (night). During this phase the telescope receives IR radiation from the Earth. Depending on the spacecraft orientation and on the length of the occultation, HST may be more or less heated. The two cycles determine the amount of thermal excursion that HST suffers during one orbit.

The fluctuations in the HST thermal environment induce variations up to several microns in the distance between HST primary and secondary mirrors. These changes translate into changes in the telescope focus, and reflect into changes in the shape and the sharpness of the PSF of the various instruments.

To quantify the spatial variability of UVIS PSFs, for each of the 36 exposures acquired in the F606W filter we measured the total flux within 1, 2, 3, 4, 5, 6, 7, 8, and 9 pixel radius, with respect to the flux measured within 10 pixels for each of the 9x10 PSF models. Figure 3 summarizes our findings. Each panel (labelled from 1 to 36) shows the relative flux variation for each of the 90 PSF modelsas a function of the aperture radius. The relative flux depends on the position on the detector. In addition, changes with time are also noticable. For example in panel 36 the flux measured within a three pixel aperture varies between 77% and 85% of the flux measured in a 10 pixel aperture, while in plot 3 the same aperture contains between 81% and 86% of the flux measured within the 10 pixel aperture. The effect becomes even more severe for smaller apertures. A similar effect was noted by Dressel (2012), who studied the variability of PSFs observed 39 times per orbit over 8 orbits using a 512×512 pixel sub-array near the center of the detector.

Because of the tilt of the camera, the UVIS channel is affected by astigmatism. This effect becomes quite evident when the telescope is far from its optimal focus, and the PSF in the upper left corner of the detector becomes elongated (Sabbi 2009b). To verify how well the shape of the PSF correlates with the focus of the UVIS camera we measured the residual flux that remains in the upper-left corner of the detector, after we subtracted an average, spatially constant PSF from the grid of 9x10 PSF models derived for each exposure.

In the upper left corner the residuals typically show two peaks and two hollows. The orientation and intensity of peaks and hollows change as a function of focus. To quantitatively evaluate these changes in each exposure, we measured the residual flux in four regions around the center of the upper-left PSF (see Figure 4).

We used the *HST* Focus Model (http://www.stsci.edu/hst/observatory/focus/FocusModel) to obtain an estimate (in micron) of the telescope focal length for each observation relative to the best focus. The correlation between *HST* focus and the residual flux in the upper-left corner PSF is shown in Figure 5. This plot shows that when the focus is negative, the PSF in the upper-left corner is elongated in the lower-left/upper-right direction, it is roughly circular when the focus is close to 0 and becomes elongated in the upper-left/lower-right direction when the focus is positive, as expected in the case of astigmatism. Similar changes, although less noticeable, are found for the other four corners.

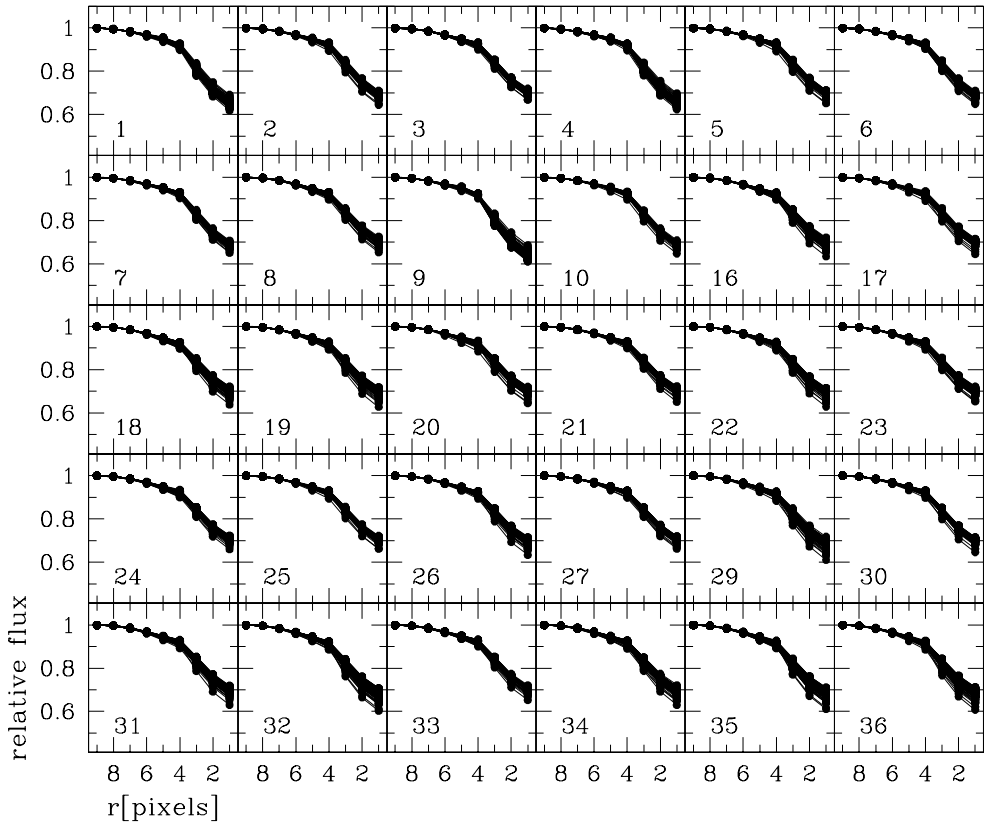

Figure 3: Ratio between the flux measured in a 1, 2, 3, 4, 5, 6, 7, 8, and 9 pixel aperture compared to the flux measured in a 10 pixel radius aperture for each of the 90 PSFs (black dots) of each exposures (panels 1 to 36). Panels 11, 12, 13, 14, 15, and 28 refer to exposures that have been compromised because of the lost of the Guide Star, and have been discarded.

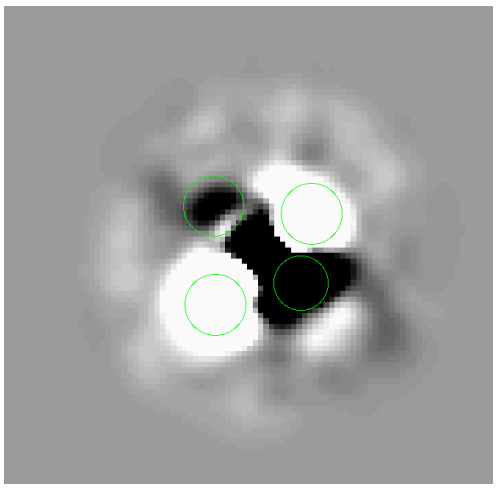

Figure 4: Example of the residual PSF in the upper left corner of the UVIS channel. The four green circles mark the region where the residual flux was measured in each image to investigate the relation between focus and PSF shape.

Table 2 reports, for each image, the ratio between the flux measured in a 3 and a 10 pixel radius apertures averaged over all the 90 PSFs of the image (3rd and 8th columns), the minimum (columns 4 and 9) and maximum difference (columns 5 and 10) as a function of the telescope focus. When the focus is close to its optimal value (0) over the entire image the PSF is sharper, and the average relative flux is higher and the dispersion is small. When the telescope is far from its optimal focus, the PSFs are broader, and are characterized by a larger dispersion.

Obs	Focus	F_{Ave}	F_{Min}	F_{Max}	Obs	Focus	F_{Ave}	F_{Min}	F_{Max}
1	4.6	0.804	0.778	0.878	21	-0.5	0.842	0.803	0.856
2	1.9	0.832	0.794	0.852	22	-1.1	0.834	0.785	0.850
3	0.1	0.842	0.811	0.855	23	-0.4	0.839	0.798	0.856
4	3.7	0.808	0.780	0.841	24	0.3	0.844	0.809	0.855
5	0.3	0.838	0.797	0.853	25	-0.5	0.843	0.803	0.857
6	1.2	0.832	0.801	0.851	26	-1.3	0.835	0.788	0.850
7	0.9	0.830	0.802	0.849	27	0.5	0.843	0.809	0.855
8	-1.7	0.842	0.804	0.856	29	-3.6	0.825	0.770	0.850
9	2.4	0.794	0.774	0.832	30	-0.2	0.840	0.798	0.852
10	1.6	0.833	0.794	0.848	31	-1.4	0.837	0.786	0.853
16	-0.8	0.836	0.788	0.853	32	-3.3	0.820	0.762	0.843
17	-1.1	0.840	0.796	0.857	33	-3.8	0.842	0.802	0.853
18	-1.7	0.837	0.793	0.853	34	-0.1	0.834	0.787	0.851
19	-0.9	0.834	0.784	0.854	35	-2.4	0.821	0.769	0.844
20	0.5	0.839	0.790	0.853	36	-4.5	0.824	0.766	0.846

Table 2: Comparison between the telescope focus in micron and the fraction of flux measured in a 3 pixel radius aperture compare to the flux measured in a 10 pixel radius aperture. Image numbers are listed in columns 1 and 6; the value of the focus is reported in columns 2 and 7; column 3 and 8 give the relative flux, averaged over the entire image; columns 4 and 9 list the minimum frelaive flux for the image, and the maximum relative flux is listed in columns 5 and 10.

Conclusions

We used observations of the globular clusters ω Centauri in the filter F606W to investigate how the UVIS PSF changes as a function of position on the detector and of time because of the telescope breathing. We found that the dependence of the encircled PSF energy on the position on the detector and on focus becomes marginal for apertures larger than 7-8 pixels.

Changes in the telescope focus affect the shape and the sharpness of the PSF. The correlation between these variations and the focus is quite stable, thus Archival data of rich stellar fields can be used to both derive empirical models of PSFs for the UVIS detector at various wavelengths, and also to provide a correction to take into account the status of the telescope focus at the moment of the observation.

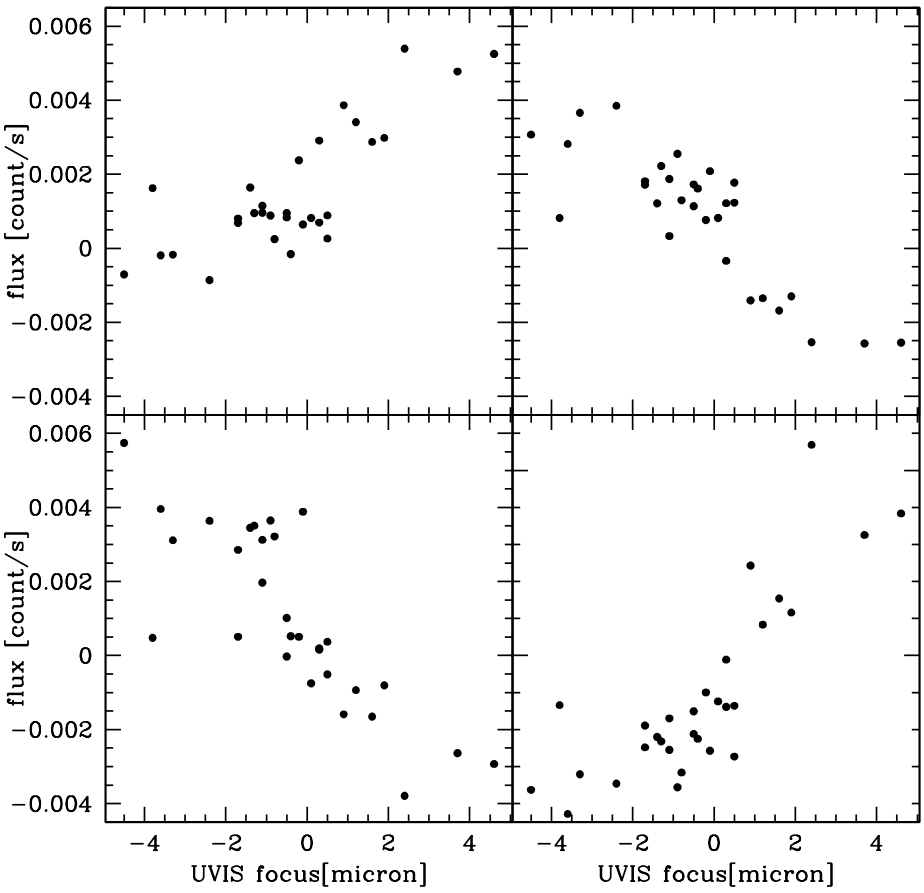

Figure 5: Residual flux in region of a PSF in the upper left corner as a function of the telescope focus. Each panel corresponds to one of the regions marked in Figure 4.

Aknowledgemt
We thanks Jay Anderson for the discussios about HST PSFs, Matt Lallo for the explanations about HST focus, and Linda Dressel for reviewing this ISR.

References

Anderson, J., Bedin, L.R., Piotto, G., Yadav, R.S., Bellini, A. 2006, A&A, 454, 1029
Bellini, A., & Bedin, L.R. 2009, PASP, 121, 1419
Bellini, A., Anderson, J, Bedin, L.R. 2010, PASP, 123, 622
Dressel 2012, "Breathing, Position Drift, and PSF Variations on the UVIS Detector", WFC3-ISR 2012-14
Kozurina-Platais, V., Cox, C., McLean, B., Petro, L., Dressel, L., Bushouse, H., Sabbi, E. 2009, "WFC3 SMOV Proposal 11444 – UVIS Geometric Distoriotion Calibration", WFC3-ISR 2009-33
Kozurina-Platais, V., & Petro, L. 2012, "WFC3/UVIS asn IR Time Dependency of Linear Geometrc Distorion over Cycle 17 and 18", WFC3-ISR 2012-03
Mack, J., Sabbi, E., & Dahel, T.2013, "Inflight Correction to the WFC3 UVIS Flat Fields", WFC3-ISR 2013 (under review)

Sabbi, E. 2009a, “WFC3 SMOV Program 11452: UVIS Flat Field Uniformity”, WFC3-ISR 2009-19
Sabbi, E. 2009b, “WFC3 SMOV Program 11798: UVIS PSF Core Modulation”, WFC3-ISR 2009-20
Sabbi, E., et al. 2009, “WFC3 Calibration using Galactic Clusters”, WFC3-ISR 2009-06
Sabbi E., Dulude, M., Martel, A.R., Baggett, S., Bushouse, H. 2009, “WFC3 UVIS Ground P-flats”, WFC3-ISR 2008-46
Wong, M. 2010, in “The 2010 STScI Calibration Workshop”, ed. S. Deustua and C. Oliveira (Baltimore: STScI), 183, “Fringing in the WFC3/UVIS Detector”